Cooperative nanomaterial system to sensitize, target, and treat tumors

Ji-Ho Park[a,b], Geoffrey von Maltzahn[c], Mary Jue Xu[c], Valentina Fogal[d], Venkata Ramana Kotamraju[e], Erkki Ruoslahti[d,e], Sangeeta N. Bhatia[c,f,g], and Michael J. Sailor[a,b,h,1]

[a]Materials Science and Engineering Program, [b]Department of Chemistry and Biochemistry, and [h]Department of Bioengineering, University of California, San Diego, La Jolla, Ca 92093, and [c]Harvard-MIT Division of Health Sciences and Technology, and [f]Electrical Engineering and Computer Science, Massachusetts Institute of Technology, Cambridge, Ma 02139, and [g]Division of Medicine, Brigham and Women's Hospital, Boston, Ma 02115, and [d]Cancer Research Center, Burnham Institute for Medical Research, 10901 North Torrey Pines Road, La Jolla, Ca 92037, and [e]Vascular Mapping Center, Burnham Institute for Medical Research at UCSB, University of California, Santa Barbara, Santa Barbara, Ca 93106

Edited by Mark E. Davis, California Institute of Technology, Pasadena, CA, and approved November 16, 2009 (received for review September 2, 2009)

A significant barrier to the clinical translation of systemically administered therapeutic nanoparticles is their tendency to be removed from circulation by the mononuclear phagocyte system. The addition of a targeting ligand that selectively interacts with cancer cells can improve the therapeutic efficacy of nanomaterials, although these systems have met with only limited success. Here, we present a cooperative nanosystem consisting of two discrete nanomaterials. The first component is gold nanorod (NR) "activators" that populate the porous tumor vessels and act as photothermal antennas to specify tumor heating via remote near-infrared laser irradiation. We find that local tumor heating accelerates the recruitment of the second component: a targeted nanoparticle consisting of either magnetic nanoworms (NW) or doxorubicin-loaded liposomes (LP). The targeting species employed in this work is a cyclic nine-amino acid peptide LyP-1 (Cys-Gly-Asn-Lys-Arg-Thr-Arg-Gly-Cys) that binds to the stress-related protein, p32, which we find to be upregulated on the surface of tumor-associated cells upon thermal treatment. Mice containing xenografted MDA-MB-435 tumors that are treated with the combined NR/LyP-1LP therapeutic system display significant reductions in tumor volume compared with individual nanoparticles or untargeted cooperative system.

cancer therapy | gold nanorods | liposomes | magnetic nanoworms | protein expression

In the past few decades, nanomaterials have played a propitious role in delivering therapeutic molecules effectively to diseased sites. In addition to their role as effective carriers of conventional therapeutic drugs, nanoscale materials can be harnessed to damage or destroy malignant tissues by converting external electromagnetic energy into heat (1–6). Furthermore, most nanomaterial surfaces can be decorated with targeting ligands, enhancing their ability to home to diseased tissues through multivalent interactions with tissue-specific receptors (7). Targeted liposomes (8, 9), micelles (10, 11) and dendrimers (12, 13) incorporated with therapeutic molecules have displayed impressive anticancer effects in animal studies, and these nanomaterials are considered to be close to clinical translation due to their biocompatibility. In spite of these merits, nanotechnology-based cancer therapies have been slow to reach the clinic compared to conventional cancer therapies such as small molecule drugs, whole-body or local hyperthermia, and radiation.

Tumorigenesis is a multistep process that requires expression of tumor-associated proteins and suppression of proteins controlling normal cell growth (14). Many of the identified tumor-specific proteins have been exploited to develop powerful antibody, aptamer, peptide, and small molecule-based ligands for targeting of diagnostic or therapeutic agents (15). Ligand-directed targeting of therapeutic nanomaterials has been widely pursued to improve therapeutic efficacy, although limitations imposed by the tumor microenvironment, such as restricted transvascular transport and receptor accessibility, have prevented realization of their full capabilities. Although the porous microstructure of tumor blood vessels is favorable for nonspecific infiltration of circulating nanomaterials into the extravascular region of the tumor (16), extravasated nanomaterials are generally deposited close to the vessels, resulting in a highly heterogeneous distribution of therapeutic agents in the tumor.

Hyperthermia has been reported to not only improve nanoparticle extravasation in tumors, (17) but it also can selectively damage neoplastic cells to activate immunological processes and induce expression of particular proteins (18). Widely used in the clinical setting in concert with chemotherapy and radiotherapy (19, 20), tumor-specific hyperthermia would be a powerful tool to manipulate tumor microenvironments in order to enhance the interactions between cancerous tissues and therapeutic agents. However, hyperthermia methods in clinical practice lack intrinsic specificity for tumor tissues, requiring complex implementation strategies and frequently resulting in exposure of large volumes of normal tissues to hyperthermic temperatures alongside tumors. We hypothesized that gold nanorods (NRs), passively accumulated in tumors via their fenestrated blood vessels, could be used to precisely heat tumor tissues by amplifying their absorption of otherwise benign near-infrared energy (2, 6) and allow the recruitment and more effective penetration of a second, specifically targeted nanoparticle. Thus, in this work, we demonstrate a cooperative nanomaterials system, wherein NRs accumulated in a tumor photothermally activate the local microenvironment to amplify the targeting efficacy of two types of targeted, circulating nanoparticles: magnetic nanoworms (NWs) and liposomes (LPs) loaded with the anticancer drug doxorubicin (DOX) (Fig. 1*A*).

Results

The first stage of the cooperative nanoparticle system, the photothermally-heated gold nanorods, has already been demonstrated by our group (6). Polyethylene glycol (PEG)-coated NRs with a maximum optical absorption of 800 nm are found to accumulate passively in a MDA-MB-435 xenograft tumor. Effective in vivo photothermal heating of the tumor is achieved by application of NIR irradiation (810 nm, ~0.75 W/cm^2) from a diode laser (Fig. 1*B*).

A cyclic nine-amino acid peptide (Cys-Gly-Asn-Lys-Arg-Thr-Arg-Gly-Cys), referred to as LyP-1, was chosen as the targeting

Author contributions: J.-H.P., G.v.M., E.R., S.N.B., and M.J.S. designed research; J.-H.P., G.v.M., M.J.X., V.F., E.R., S.N.B., and M.J.S. analyzed data; J.-H.P. and M.J.S. wrote the paper; J.-H.P., G.v.M., M.J.X., and V.F. performed research; and V.R.K. contributed new reagents/analytic tools.

The authors declare no conflict of interest.

This article is a PNAS Direct Submission.

[1]To whom correspondence should be addressed: E-mail: msailor@ucsd.edu.

This article contains supporting information online at www.pnas.org/cgi/content/full/0909565107/DCSupplemental.

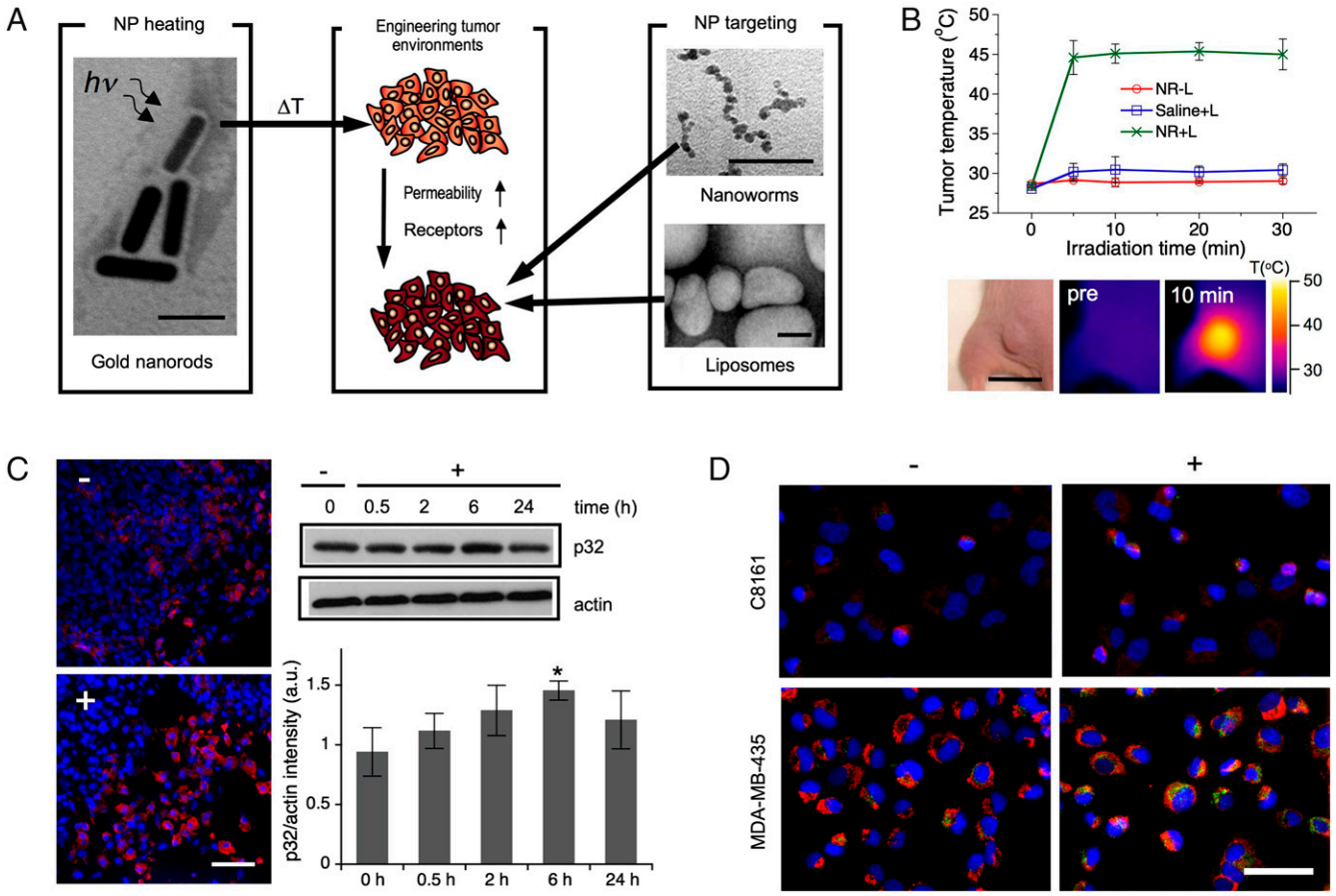

Fig. 1. Characterization of the components of cooperative nanosystems. (*A*) Schematic showing the components of the two cooperative nanomaterials systems used in this study. The first component consists of gold nanorods (NR), which act as a photothermal sensitizer. The second component consists of either magnetic nanoworms (NW), or doxorubicin-loaded liposomes (LP). Irradiation of the NR with a NIR laser induces localized heating that stimulates changes in the tumor environments. The NW or LP components decorated with LyP-1 tumor targeting peptides bind to the heat-modified tumor environments more efficiently than to the normal tumor environments. Transmission electron microscope images of all three components are shown. Scale bars indicate 50 nm. (*B*) Temperature changes induced by localized laser irradiation (+L) of mice injected with NR alone (no NW or LP). Tumor-bearing mice were injected intravenously with either PEGylated NRs (NR) or saline (saline). Trace labeled "NR-L" is a control where NRs were injected but the tumor was not irradiated. Data and images obtained 72 h postinjection; infrared thermographic maps of average tumor surface temperature were obtained after laser exposure for the indicated times. Scale bar indicates 1 cm. (*C*) Effect of heating time on p32 expression in MDA-MB-435 xenograft tumor. Tumor in an athymic (nu/nu) mouse was heated at 45 °C for 30 min in a water bath. Images at left show cell surface p32 immunostaining of tumor sections 6 h posttreatment. Symbols + and − indicate with and without heating, respectively. Scale bar indicates 50 μm. At right are Western blot results for p32 relative to β-actin control. * indicates $P < 0.05$ for 0 h and 6 h intensity ratio ($n = 3 \sim 4$). Brightness and contrast have been adjusted across the whole image. (*D*) Fluorescence microscope images of C8161 or MDA-MB-435 cells probing in vitro cellular binding and internalization of LyP-1-conjugated Cy5.5-labeled magnetic nanoworms (LyP1NWs, in green) upon heating to 45 °C. Samples were incubated for 20 min at 37 °C (–) or 45 °C (+) and then held at 37 °C for an additional 2 h. Cell nuclei and p32 stained with 4′-6-diamidino-2-phenylindole (DAPI, *Blue*), and anti-p32 antibody followed by Alexa Fluor® 594 goat antirabbit IgG antibody (*Red*), respectively. Scale bar indicates 50 μm. All error bars indicate standard deviations from ≥3 measurements. Brightness and contrast have been adjusted across the whole image.

ligand based on a screen of several tumor targeting peptides in MDA-MB-435 xenograft tumors, which showed enhanced LyP-1 accumulation in the heated tumors. The LyP-1 peptide has been reported to selectively recognize lymphatics and tumor cells in certain tumor types and subsequently inhibit tumor growth (21, 22). Recently, it was found that the p32 or gC1qR receptor, whose expression is elevated on the surface of tumor-associated cells undergoing stress, is the target molecule for the LyP-1peptide (23). Thus, we investigated whether the enhanced targeting of LyP-1 relates to upregulation of p32 receptors in the heated tumor.

We first tested the level of p32 expression in MDA-MB-435 xenografts as a function of time postheat treatment. An externally measured temperature of 45 °C was chosen for the laser heat treatment based on a preliminary screen of temperature dependent nanoparticle accumulation. It has been reported that cancer cells are most vulnerable to hyperthermia, chemotherapeutics, or a combined therapy above temperatures of 43 °C (18, 20). Expression of p32 on the MDA-MD-435 tumors was slightly upregulated 6 h after heat treatment, which then returned to almost normal levels 24 h posttreatment (Fig. 1*C*). Compared with the MDA-MB-435 tumors, less significant changes in the level of heat-mediated p32 expression were observed on C8161 tumors, known as the tumor type that expresses a considerably less amount of p32 compared to MDA-MB-435 tumor (23), over a 24 h period postheating (Fig. S1). Expression of p32 in cultured cells upon heat treatment exhibited a pattern similar to the in vivo xenograft results; the extent of p32 expression on C8161 cells (and cell surfaces) was less than that observed with MDA-MB-435 cells (Fig. S2).

We next investigated the interaction of nanoparticles decorated with LyP-1 peptides with cancer cells upon heat treatment. An optimized formulation of NWs was prepared as previously described (24, 25), and coated with LyP-1 peptides via PEG linkers (~40 peptides per nanoworm). Significant quantities of the LyP-1 peptide-conjugated NWs (LyP1NWs) were internalized

into heated MDA-MB-435 cells relative to unheated cells. In contrast, the C8161 cells displayed lower heat-mediated internalization than the MDA-MB-435 cells (Fig. 1*d*). The colocalization of p32 receptors and LyP1NW was clearly observed in MDA-MB-435 cells, suggesting that the binding and internalization of LyP1NWs are mediated by p32 receptors on the surface of MDA-MB-435 cells. The lack of interaction of LyP1NWs with C8161 cells is presumed to be due to insufficient availability of p32 receptors on the cell surface (Fig. S2). As expected, control NWs exhibited no interaction in either cell type, regardless of the heat treatment (Fig. S3).

The possibility of selective homing of LyP1NWs to heated xenograft tumors in vivo was then tested. Similar to the in vitro results, targeting of LyP1NWs to heated MDA-MB-435 tumors was prominent relative to unheated tumors, since the ability of LyP1NWs to home to heated C8161 tumors was not significantly different relative to the unheated tumors (Figs. 2 and S4). Histological analysis revealed large quantities of LyP1NWs occupying vessel structures that were not colocalized with the blood vessel stain, consistent with the previously reported affinity of LyP-1 for lymphatics (21). In both types of tumors, most of the observed LyP1NWs were either colocalized with p32 receptors or distributed in the extravascular region of the heated tumors. Additionally, the distribution of control NWs in tumors did not correlate with the p32 receptor distribution, even though significant quantities of NWs were observed in the heated tumors. Furthermore, histological images of tumors for which LyP1NWs were administered immediately after heat treatment were similar to those for which LyP1NWs were injected right before heat treatment (Fig. S5), suggesting that prominent targeting of LyP1NWs on the individual cells of heated tumors can be attributed mainly to their binding to the p32 receptors, not the simultaneous hyperthermia.

Having verified temperature-induced amplification of nanoparticle targeting to tumor cells in vitro and to xenografted tumors in vivo, we next evaluated in vitro photothermal-assisted cytotoxicity of targeted therapeutic carriers. Liposomes constructed from lipids that are not thermally sensitive were prepared and loaded with the anticancer drug doxorubicin (DOX) (26). The LyP-1 peptide-conjugated DOX liposomes (LyP1LPs) displayed greater levels of cytotoxicity toward MDA-MB-435 cells relative to control DOX liposomes (DOX concentration > 10 ugDOX/mL in both experiments). Enhanced cytotoxicity was observed for heat-treated (45 °C) samples, whereas the measured difference in cytotoxicity at 37 °C was insignificant (Fig. 3*A* and 3*B*). The increased cytotoxicity of LyP1LPs toward heat-treated cells is ascribed to a combination of hyperthermal chemotherapy and targeting to (upregulated) receptor proteins. Although it was reported that LyP-1 peptide itself has a therapeutic effect (22), the peptide amount on the particles is much less than was needed for the antitumor activity. By contrast, the heat-induced cytotoxicity of LyP1LPs toward C8161 melanoma cells was significantly less pronounced; this is attributed to lower levels of expression of p32 on the C8161 cellular surface and higher resistance to DOX, relative to MDA-MB-435 cells (Fig. S6).

Finally, the therapeutic efficacy of the complete cooperative nanomaterials system was tested on a xenograft mouse cancer model. Twenty-four h posttreatment, targeting efficacy of LyP1LPs was significantly larger in the photothermally engineered tumors than in the normal tumors and than that of control LPs (Fig. 4*A* and *B*). The results clearly show that targeted LPs display greater accumulation in the engineered tumors and deliver more encapsulated DOX payload relative to untargeted LPs. By contrast, in the normal (unheated) tumor environment, both LP formulations show relatively low levels of accumulation (Figs. 4*A* and S7). Additionally, in order to achieve therapeutic effects in the unheated tumor, multiple administrations of relatively high doses of LPs are required (Fig. S8). However, addition of the targeting ligand LyP-1 to the LP formulation slows tumor growth, in accord with previous work (27).

As mentioned above, hyperthermia in the temperature range ~43 °C has been shown to selectively damage malignant cells relative to normal cells (18). Similarly, the increased temperature in the tumor produced by NR-mediated photothermal heating slows tumor growth in vivo, although it does not reduce tumor volume (Fig. S9). However, tumors (or tumor cells) whose local microenvironment has been engineered by NR-mediated heating are more vulnerable to attack by therapeutic nanoparticles (Fig. 4*C* and 4*D*). Combined with NR-mediated photothermal engineering, a single injection of therapeutic nanoparticles at a

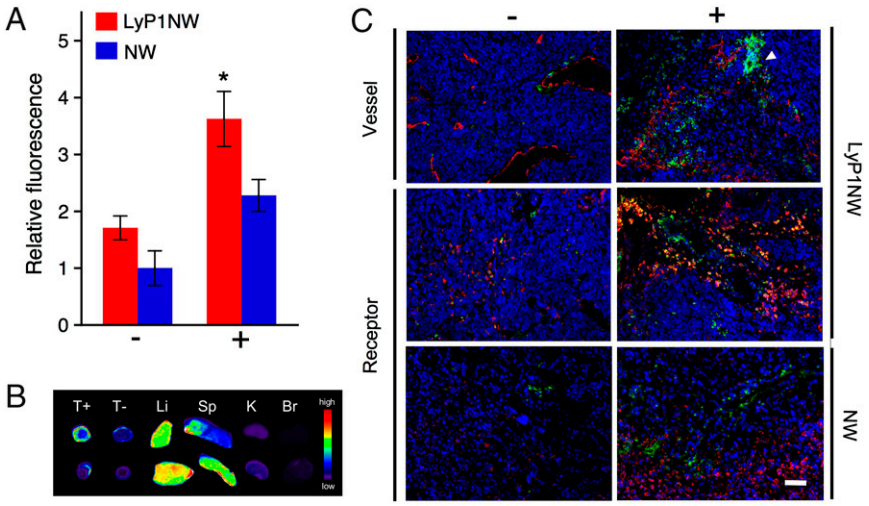

Fig. 2. Temperature-induced amplification of in vivo tumor targeting. (*A*) Fluorescence intensity from Cy7-labeled LyP-1-conjugated magnetic nanoworms (LyP1NW) and Cy7-labeled control nanoworms (NW) in MDA-MB-435 tumor as a function of externally applied heat (30 min). Heated at (45 °C) and unheated (37 °C) samples indicated with (+) and (–), respectively. The tissues were collected from the mice 24 h postinjection; NIR fluorescence images use Cy7 channel. * indicates $P < 0.05$ ($n = 3 \sim 4$). (*B*) Fluorescence image of major organs from the mice in (*A*). T+, T–, Li, Sp, K, and Br indicate heated tumor, unheated tumor, liver, spleen, kidney, and brain, respectively. (*C*) Histological analysis of LyP1NW or NW distribution in MDA-MB-435 tumors with (+) or without (–) application of external heat. *Green* indicates NWs (labeled with Cy 5.5). Cellular stains same as in Fig. 1*D*, blood vessels stained with CD31 followed by Alexa Fluor® 594 goat antirat IgG. Arrowhead indicates a lymphatic vessel structure displaying a signal from the labeled LyP1NWs. Scale bar is 100 μm. Error bars indicate standard deviations from ≥3 measurements.

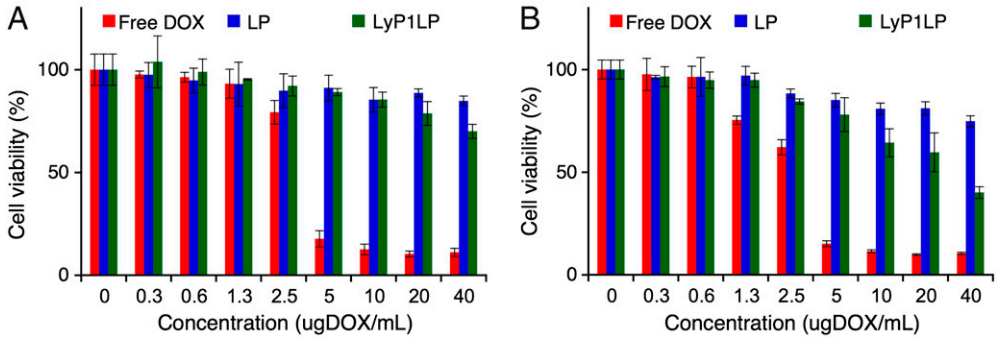

Fig. 3. Heat-mediated cytotoxicity of targeted therapeutic nanoparticles in vitro. (*A* and *B*) Temperature-induced cytotoxicity of various therapeutic molecule or nanoparticle formulations toward MDA-MB-435 human carcinoma cells by MTT assay. The cells were treated with free DOX, control DOX-containing liposomes (LP), or LyP-1-conjugated, DOX-containing liposomes (LyP1LP) with the indicated concentrations of DOX. Samples incubated at 37 °C (*A*) or 45 °C (*B*).

relatively low therapeutic dose (3 mgDOX/kg) is able to achieve significant tumor regression or elimination, which has not been observed in this tumor model with previous targeted therapies even with multiple high doses (27, 28). For all the treatments studied in this work, no significant loss of body mass was observed.

Discussion

This study demonstrates that the appropriate combination of nanomaterials currently under investigation in cancer therapy can significantly enhance therapeutic efficacy relative to the individual components. Site-specific photothermal heating of NRs can engineer the local tumor microenvironment to enhance the accumulation of therapeutic targeted liposomes, which increases the overall hyperthermal and chemotherapeutic tumor-destroying effects. This cooperative nanosystem holds clinical relevance because gold salts (for rheumatoid arthritis therapies) (29) and doxorubicin-containing liposomes (Doxil®) have been approved for clinical use, and local hyperthemia is a well-established means of destroying diseased tissues in the human body. Although the liposomes in this study are similar to Doxil®, it should be pointed out that the gold nanorod and iron-oxide nanoworm formulations used in the study are somewhat distinct from clinically approved gold or iron oxide materials. Because they are quite bioinert, much work needs to be done to investigate the long-term fate and biosafety of systemically administered gold nanorods in the human body. Cooperative, synergistic therapies using dual or multiple nanomaterials could significantly reduce the required

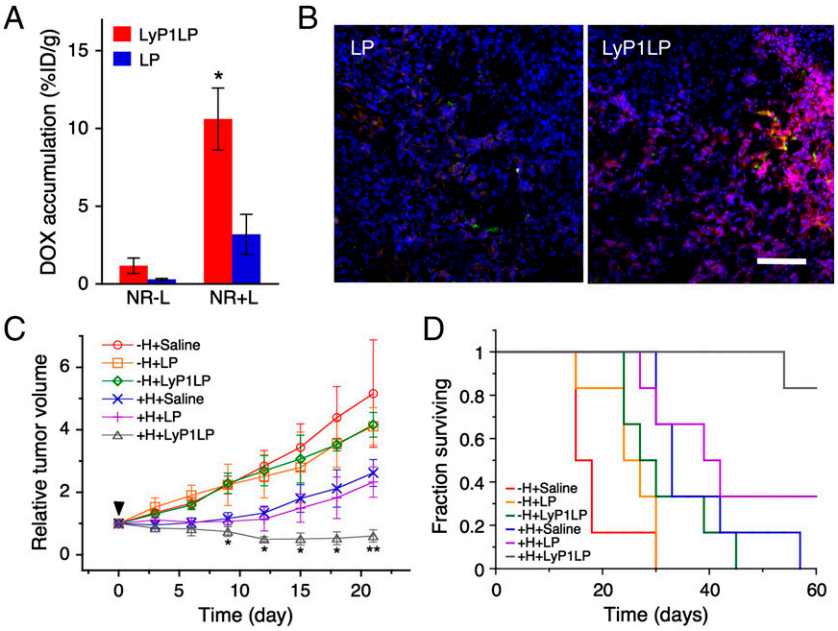

Fig. 4. Successful antitumor therapy using cooperative nanosystem, demonstrated in mice bearing MDA-MB-435 tumors. (*A*) Quantification of in vivo accumulation of DOX in tumors as a function of NR-mediated laser heating of LyP-1-conjugated liposomes (LyP1LP) or control liposomes that contain no targeting peptide (LP). NR + L and NR − L indicate mice containing gold nanorods that were or were not subjected to laser treatment, respectively. Amount of DOX present quantified by fluorescence microscopy to yield a percentage of injected dose per tissue mass. * indicates $P < 0.05$ ($n = 3 \sim 4$). (*B*) Histological analysis of DOX distribution in tumors from the mice in (*A*) who were subjected to NR-mediated thermal therapy showing the distribution of nanoparticles (Alexa Fluor® 488 label on control liposome and 5(6)-carboxyfluorescein (FAM) label on LyP-1, *Green*) and DOX (*Red*). Nuclei stained with DAPI (*Blue*). Scale bar is 100 μm. (*C*) Change in tumor volume of different treatment groups containing bilateral MDA-MB-435 xenograft tumors. 72 h postinjection of gold nanorods (NR, 10 mgAu/kg), mice were injected with a single dose of saline, control liposomes (LP), and LyP-1-conjugated liposomes (LyP1LP). "+H (Hyperthermia)" denotes one of the two tumors in the animal that was irradiated with the NIR laser. The tumor not irradiated is indicated as "−H". Tumor volumes monitored every 3 d postirradiation. Error bars indicate standard deviations from ≥3 measurements. * indicates $P < 0.05$ and ** indicates $P < 0.02$ for +H + LyP1LP sample and all other treatment sets ($n = 4 \sim 6$). (*D*) Survival rate in different treatment groups after a single dose (3 mgDOX/kg) into mice ($n = 6$) containing single MDA-MB-435 xenograft tumors. Error bars indicate standard deviations from ≥3 measurements.

dose of anticancer drugs, mitigating toxic side effects, and more effectively eradiating drug-resistant cancers.

Materials and Methods

Preparation of Gold Nanorod, Magnetic Nanoworm, and Doxorubicin Liposomes. Gold nanorods (NRs) were purchased from Nanopartz with a peak plasmon resonance at 800 nm and coated with polyethelene glycol (PEG) molecules [HS-PEG(5k)]. Superparamagnetic, dextran-coated iron-oxide nanoworms (NWs) with a longitudinal size of ~70 nm were synthesized with the published procedure (24), and derivatized with near-infrared (NIR) fluorophore, Cy5.5/Cy7-NHS. For control NWs, partially Cy5.5/Cy7-labeled aminated NWs were coated with a PEG molecule [NHS-PEG(5k)]. For LyP-1-conjugated NWs (LyP1NWs), LyP-1 peptides with extra cysteine were attached to partially Cy5.5/Cy7-labeled aminated NWs via a PEG crosslinker [NHS-PEG(5k)-MAL]. Control liposomes (LPs), with no functional group were prepared from hydrogenated soy sn-glycero-3-phosphocholine (HSPC), cholesterol, and 1,2-distearoyl-snglycero-3-phosphoethanolamine-N-polyethylene glycol 2000 [DSPE-PEG(2k)] (75:50:6 mol ratio) by lipid film hydration and membrane (100 nm) extrusion (30). Incorporation of DOX was achieved using the pH gradient-driven protocol (31). For LyP-1-conjugated LPs (LyP1LPs), LPs with maleimide groups were prepared from HSPC, cholesterol, DSPE-PEG(2k), and DSPE-PEG(2k)-MAL (75:50:6:6 mol ratio). LyP-1 peptides with an extra cysteine were attached to maleimide-terminated LPs in PBS. LPs were intravenously injected in vivo to ensure control LPs and LyP1LPs exhibited similar circulation times (blood half-lives for both: ~3 hrs).

In Vitro Cellular Fluorescence Imaging. The cells were treated with 80 ugFe/mL of Cy5.5 labeled control NWs or LyP1NWs per well for 20 min at 37 °C or 45 °C in the presence of 10% FBS and incubated for an additional 2 h at 37 °C in the presence of 10% FBS. The cells were then rinsed three times with cell medium, fixed, stained, and imaged by fluorescence microscopy.

In Vivo Temperature-Induced Tumor Targeting of Magnetic Nanoworms. Mice bearing bilateral tumors (MDA-MB-435 human carcinoma or C8161 human melanoma) were intravenously injected with Cy7-labeled LyP1NWs or NWs and one tumor of the mouse was immediately heated at 45 °C for 30 min in a temperature-controlled water bath. At 24 h postinjection, the tissues were harvested and the Cy7 fluorescence in tissues were imaged using NIR fluorescence imaging system (LI-COR Odyssey).

In Vitro Temperature-Induced Cytotoxicty of Therapeutic Nanoparticles. Cells were treated with free DOX, control LPs, or LyP1LPs with different concentrations at 37 °C or 45 °C for 20 min (in cell incubator) and then incubated for an additional 4 h at 37 °C. The cells were rinsed with cell medium three times, and then further incubated for 44 h at 37 °C. The cytotoxicity of free DOX, control LPs, or LyP1LPs was evaluated using MTT assay (Invitrogen). Cell viability was expressed as the percentage of viable cells compared to controls (cells treated with PBS).

In Vivo Tumor Targeting of Therapeutic Nanoparticles by NR-Mediated Photothermal Heating. Mice bearing bilateral MDA-MB-435 human carcinoma tumors were intravenously injected with NRs (10 mgAu/kg). At 72 h postinjection of NR, control LPs, or LyP1LPs (3 mgDOX/kg) were systemically administered and the tumor in one flank was irradiated with NIR-light (~0.75 W/cm^2 and 810 nm) for 30 min, maintaining an average tumor surface temperature at ~45 °C under infrared thermographic observation. At 24 h postinjection of liposomes, doxorubicin fluorescence in the homogenized tumors was analyzed.

In Vivo Therapeutic Studies. To study the effect of photothermal treatment on tumor volumes, mice bearing bilateral MDA-MB-435 human carcinoma tumors were intravenously injected with NRs (10 mgAu/kg). At 72 h postinjection of NR, control LPs, or LyP1LPs (3 mgDOX/kg) were systemically administered and the tumor in one flank was irradiated with NIR-light (~0.70 or 0.75 W/cm^2 and 810 nm) for 30 min, maintaining average tumor surface temperature at 45 °C. Each therapeutic cohort included 4 ~ 6 mice. Tumor volume and mouse mass was measured every 3 d after the single treatment for a period of 3–4 weeks by an investigator blinded to the treatments administered. Survival rates (Kaplan Meier analyses) for the photothermal treatments were quantified using mice bearing single MDA-MB-435 human carcinoma tumors, intravenously injected with NRs (10 mgAu/kg). Control LPs or LyP1LPs (3 mgDOX/kg) were systemically administered 72 h postinjection and one of the tumor-bearing flanks was irradiated with NIR-light (~0.75 W/cm^2 and 810 nm) for 30 min, maintaining average tumor surface temperature at ~45 °C. Each therapeutic cohort included six mice. Tumor volume and mouse mass was measured every 3 d after the single treatment for a period of 9 weeks by an investigator blinded to the treatments administered. Mice were sacrificed when tumors exceeded 500 mm^3. Student's *t* test was used for statistical analysis of the results.

The experimental procedures are described in more detail in *SI Materials and Methods*.

ACKNOWLEDGMENTS. The authors thank Edward Monosov in the Burnham Institute of Medical Research for assistance with TEM analysis. This work was supported by the National Cancer Institute of the National Institutes of Health through Grants U54 CA119335 (UCSD CCNE), 5-R01-CA124427 (BRP), and U54 CA119349 (MIT CCNE). M.J.S., S.N.B., and E.R. are members of the Moores UCSD Cancer Center and the UCSD NanoTUMOR Center. J.-H.P. thanks the Korea Science and Engineering Foundation for a Graduate Study Abroad Scholarship.

1. Hirsch LR, et al. (2003) Nanoshell-mediated near-infrared thermal therapy of tumors under magnetic resonance guidance. *Proc Natl Acad Sci USA*, 100:13549–13554.
2. Huang X, El-Sayed IH, Qian W, El-Sayed MA (2006) Cancer cell imaging and photothermal therapy in the near-infrared region by using gold nanorods. *J Am Chem Soc*, 128 (6):2115–2120.
3. Jain PK, Lee KS, El-Sayed IH, El-Sayed MA (2006) Calculated absorption and scattering properties of gold nanoparticles of different size, shape, and composition: Applications in biological imaging and biomedicine. *J Phys Chem B*, 110(14):7238–7248.
4. Hauck TS, Jennings TL, Yatsenko T, Kumaradas JC, Chan WCW (2008) Enhancing the toxicity of cancer chemotherapeutics with gold nanorod hyperthermia. *Adv Mater*, 20:3832–3838.
5. Diagaradjane P, et al. (2008) Modulation of in vivo tumor radiation response via gold nanoshell-mediated vascular-focused hyperthermia: Characterizing an integrated antihypoxic and localized vascular disrupting targeting strategy. *Nano Lett*, 8(5):1492–1500.
6. Maltzahn Gv, et al. (2009) Computationally-guided photothermal tumor therapy using long-circulating gold nanorod antennas. *Cancer Res*, 69:3892–3900.
7. Mammen M, Choi SK, Whitesides GM (1998) Polyvalent interactions in biological systems: Implications for design and use of multivalent ligands and inhibitors. *Angew Chem Int Ed*, 37:2755–2794.
8. Hood JD, et al. (2002) Tumor regression by targeted gene delivery to the neovasculature. *Science*, 296:2404–2407.
9. Murphy EA, et al. (2008) Nanoparticle-mediated drug delivery to tumor vasculature suppresses metastasis. *Proc Natl Acad Sci*, 105:9343–9348.
10. Torchilin VP, Lukyanov AN, Gao Z, Papahadjopoulos-Sternberg B (2003) Immunomicelles: Targeted pharmaceutical carriers for poorly soluble drugs. *Proc Natl Acad Sci USA*, 100:6039–6044.
11. MacDiarmid JA, et al. (2009) Sequential treatment of drug-resistant tumors with targeted minicells containing siRNA or a cytotoxic drug. *Nat Biotechnol*, 27:643–651.
12. Kukowska-Latallo JF, et al. (2005) Nanoparticle targeting of anticancer drug improves therapeutic response in animal model of human epithelial cancer. *Cancer Res*, 65:5317–5324.
13. Patri AK, Kukowska-Latallo JF, James R, Baker J (2005) Targeted drug delivery with dendrimers: Comparison of the release kinetics of covalently conjugated drug and non-covalent drug inclusion complex. *Adv Drug Deliver Rev*, 57:2203–2214.
14. Hanahan D, Weinberg RA (2000) The hallmarks of cancer. *Cell*, 100:57–70.
15. Weissleder R (2006) Molecular Imaging in Cancer. *Science*, 312:1168–1171.
16. Jain RK (1999) Transport of molecules, particles, and cells in solid tumors. *Annu Rev Biomed Eng*, 1:241–263.
17. Kong G, Braun RD, Dewhirst MW (2000) Hyperthermia enables tumor-specific nanoparticle delivery: Effect of particle size. *Cancer Res*, 60:4440–4445.
18. Overgaard J (1977) Effect of hyperthermia on malignant cells in vivo. *Cancer*, 39:2637–2646.
19. Suit HD, Gerweck LE (1979) Potential for hyperthermia and radiation therapy. *Cancer Res*, 39:2290–2298.
20. Bull JMC (1984) An update on the anticancer effects of a combination of chemotherapy and hyperthermia. *Cancer Res*, 44:4853s–4856s.
21. Laakkonen P, Porkka K, Hoffman JA, Ruoslahti E (2002) A tumor-homing peptide with a targeting specificity related to lymphatic vessels. *Nat Med*, 8:751–755.
22. Laakkonen P, et al. (2004) Antitumor activity of a homing peptide that targets tumor lymphatics and tumor cells. *Proc Natl Acad Sci USA*, 101:9381–9386.
23. Fogal V, Zhang L, Krajewski S, Ruoslahti E (2008) Mitochondrial/cell-surface protein p32/gC1qR as a molecular target in tumor cells and tumor stroma. *Cancer Res*, 68:7210–7218.
24. Park J-H, et al. (2008) Magnetic iron oxide nanoworms for tumor targeting and imaging. *Adv Mater*, 20:1630–1635.
25. Park J-H, et al. (2009) Systematic surface engineering of magnetic nanoworms for in vivo tumor targeting. *Small*, 5:694–700.

26. Needham D, Anyarambhatla G, Kong G, Dewhirst MW (2000) A new temperature-sensitive liposome for use with mild hyperthermia: Characterization and testing in a human tumor xenograft model. *Cancer Res*, 60(5):1197–1201.
27. Karmali PP, et al. (2009) Targeting of albumin-embedded paclitaxel nanoparticles to tumors. *Nanomedicine*, 5:73–82.
28. Arap W, Pasqualini R, Ruoslahti E (1998) Cancer treatment by targeted drug delivery to tumor vasculature in a mouse model. *Science*, 279:377–380.
29. Pincus T, et al. (2002) Evidence from clinical trials and long-term observational studies that disease-modifying anti-rheumatic drugs slow radiographic progression in rheumatoid arthritis: updating a 1983 review. *Rheumatology*, 41:1346–1356.
30. Hope MJ, Bally MB, Webb G, Cullis PR (1985) Production of large unilamellar vesicles by a rapid extrusion procedure. Characterization of size distribution, trapped volume and ability to maintain a membrane potential. *Biochim Biophys Acta Bioenerg*, 812:55–65.
31. Mayer LD, Bally MB, Hope MJ, Cullis PR (1985) Uptake of antineoplastic agents into large unilamellar vesicles in response to a membrane potential. *Biochim Biophys Acta Bioenerg*, 816:294–302.

Supporting Information

Park et al. 10.1073/pnas.0909565107

SI Text

Materials and Methods. ***Gold nanorod preparation.*** Gold nanorods (NRs) with a coating of cetyltrimethylammonium bromide (CTAB) were purchased from Nanopartz with a peak plasmon resonance at 800 nm. To replace CTAB-monolayers with polyethelyne glycol (PEG) molecules, solutions of CTAB-NRs were brought to 100 μM of 5 kDa thiol-PEG and dialyzed for 24–48 h in a 5 kDa cutoff cellulose ester membrane (SpectraPor). After dialysis, PEG-conjugated NRs were purified further with multiple rounds of centrifugation using molecular weight cutoff centrifugal filters (100 kDa cutoff, Millipore) and stored at 4 °C.

Magnetic nanoworm preparation. Superparamagnetic, dextran-coated iron oxide nanoworms (NWs) with a longitudinal size of ~70 nm were synthesized with the published procedure (1), aminated using 10% vol ammonium hydroxide, and derivatized with near-infrared (NIR) fluorophore, Cy5.5/Cy7-NHS (GE Healthcare). For control NWs, partially Cy5.5/Cy7-labeled aminated NWs were coated with a PEG molecule [NHS-PEG(5k), Nektar]. For LyP-1-conjugated NWs (LyP1NWs), LyP-1 peptides with extra cysteine were attached to partially Cy5.5/Cy7-labeled aminated NWs via a PEG crosslinker [NHS-PEG(5k)-MAL, Nektar] in phosphate buffered saline pH 7.4 (PBS). The prepared NWs were stored in PBS at 4 °C before use. The NWs were characterized via dynamic light scattering (DLS) and transmission electron microscope (TEM), and intravenously injected in vivo to ensure control NWs and LyP1NWs exhibited similar circulation times (blood half-lives for both: ~6 h).

Doxorubicin liposome preparation. Hydrogenated soy sn-glycero-3-phosphocholine (HSPC), cholesterol, and 1,2-distearoyl-snglycero-3-phosphoethanolamine-N-polyethylene glycol 2000 [DSPE-PEG(2k)], 1,2-Distearoyl-sn-Glycero-3-Phosphoethanolamine-N-[Amino(Polyethylene Glycol)2000] [DSPE-PEG-NH2 (2k)] and 1,2-Distearoyl-sn-Glycero-3-Phosphoethanolamine-N-[Maleimide(Polyethylene Glycol 2000)] [DSPE-PEG(2k)-MAL] were purchased from Avanti Polar Lipids. Doxorubicin (DOX) was purchased from Sigma Chemical Co.. For control liposomes (LPs), with no functional group were prepared from HSPC, cholesterol, and DSPE-PEG(2k) in the molar ratio of 75:50:6 by lipid film hydration and membrane (100 nm) extrusion method (2). Encapsulation of DOX into the LPs was then carried out using the pH gradient-driven loading protocol (3). For LyP-1-conjugated LPs (LyP1LPs), LPs with maleimide groups were prepared from HSPC, cholesterol, DSPE-PEG(2k), and DSPE-PEG (2k)-MAL in the molar ratio of 75:50:6. LyP-1 peptides with extra cysteine were attached to maleimide-terminated LPs in PBS. For Alexa Fluor® 488-conjugated LPs, LPs with amine groups were prepared from HSPC, cholesterol, and DSPE-PEG(2k)-NH2 in the molar ratio of 75:50:6 and conjugated with Alexa Fluor® 488-NHS (Invitrogen). The prepared LPs were stored in PBS at 4 °C before use. LPs were characterized via DLS and TEM, and intravenously injected in vivo to ensure control LPs and LyP1LPs exhibited similar circulation times (blood half-lives for both: ~3 h).

Peptide synthesis. LyP-1 peptides, a cyclic nine–amino acid peptide (Cys-Gly-Asn-Lys-Arg-Thr-Arg-Gly-Cys), were synthesized with an automatic microwaveassisted peptide synthesizer (Liberty) using standard solid-phase Fmoc/t-Bu chemistry. During synthesis, the peptides were labeled with 5(6)-carboxyfluorescein (FAM) with a 6-aminohexanoic acid spacer separating the dye from sequence. The LyP-1 peptide was synthesized with a third cysteine on the N terminus of the peptide to facilitate the nanoparticle conjugation. The peptide was chemo-selectively conjugated employing a Michael addition reaction between maleimide functional group on the particle and thiol of the third cysteine placed on the N terminus of the sequence. Details of the synthesis will be published separately.

In vivo photothermal experiments. A custom 30W, variable output 810 nm diode laser source was utilized for thermographic experiments. All experiments were conducted using a 0.8 cm diameter and ~0.75 W/cm^2 intensity beam. For photothermal tumor heating experiments, athymic (*nu/nu*) mouse bearing a MDA-MB-435 tumor in the left flank were injected intravenously with either PEGylated NRs (10 mgAu/kg) or saline. At 72 h post-injection, infrared thermographic maps of average tumor surface temperature were obtained over 30 min while irradiating left flank area of the mouse with diode laser (810 nm, 0.75 W/cm^2). Photothermal experiments were conducted under the guidance of infrared thermography (FLIR S60 camera).

Detection of protein expression by immunoblotting and immunostaining. For in vitro study, cells were seeded in 2 wells of 6-well culture plate at a density of 50–60% per well in Dulbecco's Modified Eagle's Medium (DMEM) supplemented with 10% FBS and 100 μg/mL penicillin-streptomycin 24 h before heating experiments. The cells were treated for 20 min at 37 °C or 45 °C (in cell incubator) and then incubated for an additional 2 h at 37 °C. For immunoblotting, after washing cells with PBS three times, the cells were harvested, and the cell pellets are resuspended and incubated for 30 min at 4 °C in lysis buffer [20 mmol/L Tris-HCl (pH 7.5) containing 150 mmol/L NaCl and 1% (vol) Nonidet P-40] supplemented with protease inhibitor mixture (Sigma). The cell debris was removed by centrifugation, and the protein concentration was determined with the bicinchoninic acid protein assay (Pierce). Samples of cell extracts containing 30 μg of protein were analyzed by SDS-PAGE and transferred to polyvinylidene fluoride membrane filters (Invitrogen). p32 protein was detected with anti-p32 antibody (4) and peroxidase-conjugated secondary antibody. Actin was detected with mouse monoclonal anti-actin antibody (Millipore) and peroxidase-conjugated secondary antibody. The antibody complexes on the filters were visualized with the Enhanced Chemiluminescence Plus Western Blotting Detection System (Pierce). For immunostaining, after washing cells with PBS three times, the cells were fixed with 4% paraformaldehyde for 20 min, and blocked with the solution containing 1% BSA in PBS for 30 min, incubated with 5 μg/mL anti-p32 antibody for 1 h, and then with 5 μg/mL Alexa Fluor® 594 goat anti-rabbit IgG antibody for 1 h at room temperature. The nuclei stained with DAPI were observed in blue channel (excitation at 360 nm/emission at 460 nm). The p32 were observed in Cy3.5 channel (excitation at 580 nm/emission at 620 nm).

For in vivo study, MDA-MB-435 or C8161 xenograft tumors (~0.7 cm) implanted on the flank of athymic (*nu/nu*) mice were heated at different temperature [37 °C (unheated) or 45 °C] for 30 min using temperature-controlled water bath and harvested at different time period after heating treatments. For immunoblotting, the tumors were then homogenized (Tissue Tearor, Biospec Products) and incubated for 30 min at 4 °C in the lysis buffer. The cell debris was removed by centrifugation, and the protein concentration was determined with the bicinchoninic acid protein assay (Pierce). Samples of cell extracts containing

30 μg of protein were analyzed by SDS-PAGE and transferred to polyvinylidene fluoride membrane filters (Invitrogen). p32 protein was detected with anti-p32 antibody and peroxidase-conjugated secondary antibody. Actin was detected with antiactin and peroxidase-conjugated secondary antibody. The antibody complexes on the filters were visualized with the Enhanced Chemiluminescence Plus Western Blotting Detection System (Pierce). For immunostaining, the frozen sections of tumors were fixed with aceton for 20 min, and permeabilized and blocked with the solution containing 1% BSA and 0.1% Triton X-100 in PBS for 30 min, incubated with 5 μg/mL anti-p32 antibody overnight at 4 °C, and then with 5 μg/mL Alexa Fluor® 594 goat anti-rabbit IgG antibody for 1 h at room temperature. The nuclei stained with DAPI were observed in blue channel (excitation at 360 nm/emission at 460 nm). The p32 were observed in Cy3.5 channel (excitation at 580 nm/emission at 620 nm).

In vitro cellular fluorescence imaging. Cells were maintained in Dulbecco's Modified Eagle's Medium (DMEM) supplemented with 10% fetal bovine serum (FBS) and 100 μg/ml penicillin-streptomycin. For fluorescence microscopy, the cells (3000 cells per well) were seeded into 8-well chamber slides (Lab-Tek) 24 hrs before experiments. The cells were treated with 80 μgFe/mL of Cy5.5 labeled control NWs or LyP1NWs per well for 20 min at 37 °C or 45 °C in the presence of 10% FBS and incubated for an additional 2 hr at 37 °C in the presence of 10% FBS. The cells were then rinsed three times with cell medium, fixed with 4% paraformaldehyde for 20 min, and permeabilized and blocked with the solution containing 1% bovine serum albumin (BSA) and 0.1% Triton X-100 in PBS for 30 min, incubated with 5 μg/mL anti-p32 antibody for 1 h, and then with 5 μg/mL Alexa Fluor® 594 goat anti-rabbit IgG antibody for 1 h at room temperature. The nuclei stained with 4′-6-diamidino-2-phenylindole (DAPI) were observed in blue channel (excitation at 360 nm/emission at 460 nm). The p32 were observed in Cy3.5 channel (excitation at 580 nm/emission at 620 nm). The NWs were observed in Cy5.5 channel (excitation at 680 nm/emission at 720 nm).

In vivo temperature-induced tumor targeting of magnetic nanoworms. Mice bearing bilateral MDA-MB-435 human carcinoma or C8161 human melanoma tumors were intravenously injected with Cy7-labeled LyP1NWs or NWs and one flank of the mouse (containing one of the tumors) was immediately heated at 45 °C for 30 min in a temperature-controlled water bath. At 24 hrs post-injection, the tissues were harvested and the Cy7 fluorescence in tissues were imaged in Cy7 channel (750 nm excitation/800 nm emission) using NIR fluorescence imaging system (LI-COR Odyssey Infrared Imaging System). For histological analysis, the Cy5.5-labeled LyP1NWs or NWs were injected and the tumors were harvested and sectioned. The frozen sections of tumors were fixed with acetone for 20 min, and permeabilized and blocked with the solution containing 1% bovine serum albumin (BSA) and 0.1% Triton X-100 in PBS for 30 min, incubated with 5 μg/mL anti-p32 antibody or CD31 (BD Pharmingen) overnight at 4 °C, and then with 5 μg/mL Alexa Fluor® 594 goat anti-rabbit IgG antibody or Alexa Fluor® 594 goat anti-rat IgG antibody for 1 h at room temperature, respectively. The nuclei stained with DAPI were observed in blue channel (excitation at 360 nm/emission at 460 nm). The p32 or blood vessels were observed in Cy3.5 channel (excitation at 580 nm/emission at 620 nm). The NWs were observed in Cy5.5 channel (excitation at 680 nm/emission at 720 nm).

In vitro temperature-induced cytotoxicty of therapeutic nanoparticles. Cells were maintained in Dulbecco's Modified Eagle's Medium supplemented with 10% FBS and 100 μg/mL penicillin-streptomycin. The cells were treated with free DOX, control LPs, or LyP1LPs with different concentrations at 37 °C or 45 °C for 20 min (in cell incubator) and then incubated for an additional 4 h at 37 °C. The cells were rinsed with cell medium three times, and then further incubated for 44 h at 37 °C. The cytotoxicity of free DOX, control LPs, or LyP1LPs was evaluated using MTT assay (Invitrogen). Cell viability was expressed as the percentage of viable cells compared with controls (cells treated with PBS).

In vivo tumor targeting of therapeutic nanoparticles by NR-mediated photothermal heating. Mice bearing bilateral MDA-MB-435 human carcinoma tumors were intravenously injected with NRs (10 mgAu/kg). At 72 h post-injection of NR, control LPs or LyP1LPs (3 mgDOX/kg) were systemically administered and either right or left flank (area where tumor is located) of mice was immediately irradiated with NIR-light (~0.75 W/cm^2 and 810 nm) for 30 min, maintaining average tumor surface temperature at ~45 °C under infrared thermographic observation. At 24 h post-injection of liposomes, the tissues were harvested, weighed, incubated with 500 μL of 70% EtOH, 0.3 N HCl, and homogenized (Tissue Tearor, Biospec Products) to release doxorubicin from tissues. Following homogenization, another 1 mL of 70% EtOH, 0.3 N HCl, was added to samples and they were centrifuged. Supernatants of samples were analyzed for doxorubicin fluorescence using a fluorescence microplate reader (Molecular Devices, SpectraMax GeminiEM) and compared to standard curves. For histological analysis, at 72 h post-injection of NRs, mice bearing bilateral MDA-MB-435 human carcinoma tumors were intravenously injected with Alexa Fluor® 488-labeled control LPs or LyP1LPs (3 mgDOX/kg) and either right or left flank of mice was immediately irradiated with NIR-light (~0.75 W/cm^2 and 810 nm) for 30 min, maintaining average tumor surface temperature at ~45 °C under infrared thermographic observation. At 24 h post-injection, the tumors were harvested and sectioned. The frozen sections of tumors were fixed with acetone for 20 min, and stained with DAPI. The nuclei stained with DAPI were observed in blue channel (excitation at 360 nm/emission at 460 nm). The DOX fluorescence was observed in the Cy3 channel (excitation at 540 nm/emission at 580 nm). The 5(6)-carboxyfluorescein (FAM) and Alexa Fluor® 488 on the LPs were observed in FITC channel (excitation at 490 nm/emission at 520 nm).

In vivo therapeutic studies. For tumor volume change studies without photothermal treatments, mice bearing bilateral MDA-MB-435 human carcinoma tumors were intravenously injected with NR, control LPs or Lyp1LPs (6 mgDOX/kg) at 0, 6, and 12 days. For tumor volume change studies with photothermal treatments, mice bearing bilateral MDA-MB-435 human carcinoma tumors were intravenously injected with NRs (10 mgAu/kg). At 72 h post-injection of NR, control LPs or LyP1LPs (3 mgDOX/kg) were systemically administered and either right or left flank (area where tumor is located) of mice was immediately irradiated with NIR-light at power densities of ~0.70 (for 43 °C) or ~0.75 (for 45 °C), at a wavelength of 810 nm for 30 min, maintaining average tumor surface temperature at ~43 or 45 °C under infrared thermographic observation. Each therapeutic cohort included 4–6 mice. At regular intervals (every 3 days) after single or multiple treatments, tumor volumes were measured and mice were weighed over 3 or 4 weeks by an investigator blinded to the treatments administered.

For survival rate studies with photothermal treatments by Kaplan Meier analyses, mice bearing single MDA-MB-435 human carcinoma tumors were intravenously injected with NRs (10 mgAu/kg). At 72 h post-injection of NR, control LPs or LyP1LPs (3 mgDOX/kg) were systemically administered and either right or left flank (where a tumor is located) of mice was immediately irradiated with NIR-light (~0.75 W/cm^2 and 810 nm) for 30 min, maintaining average tumor surface tempera-

ture at ~45 °C under infrared thermographic observation. Each therapeutic cohort included six mice. At regular intervals (every 3 days) after single treatments, tumor volumes were measured and mice were weighed over 9 weeks by an investigator blinded to the treatments administered. Mice were killed when tumors exceeded 500 mm^3.

All animal work was performed in accordance with the institutional animal protocol guidelines in place at the Massachusetts Institute of Technology, and it was reviewed and approved by the Institute's Animal Research Committee. Student's *t* test was used for statistical analysis of the results.

1. Park J-H, et al. (2008) Magnetic iron oxide nanoworms for tumor targeting and imaging. *Adv Mater* 20:1630–1635.
2. Hope MJ, Bally MB, Webb G, Cullis PR (1985) Production of large unilamellar vesicles by a rapid extrusion procedure. Characterization of size distribution, trapped volume and ability to maintain a membrane potential. *Biochim Biophys Acta* 812:55–65.
3. Mayer LD, Bally MB, Hope MJ, Cullis PR (1985) Uptake of antineoplastic agents into large unilamellar vesicles in response to a membrane potential. *Biochim Biophys Acta* 816:294–302.
4. Fogal V, Zhang L, Krajewski S, Ruoslahti E (2008) Mitochondrial/cell-surface protein p32/gC1qR as a molecular target in tumor cells and tumor stroma. *Cancer Res* 68:7210–7218.

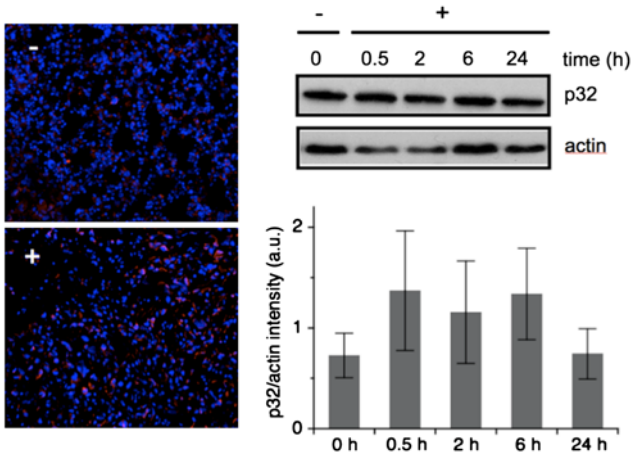

Fig. S1. Effect of p32 expression in C8161 xenograft tumor on increased temperature and heating time in vivo. A C8161 xenograft tumor on athymic (*nu/nu*) mouse was heated at 45 °C for 30 min using temperature-controlled water bath. At 6 h after heating treatment, the tumor sections were imaged for analysis of p32 expression by immnostaining (*Left*). At different time period after heating treatment, the tumors were harvested and processed for analysis of p32 expression by western blot (*Right*). β-actin was used as a control. Symbols – and + indicate no heating (37 °C) and heating (45 °C), respectively. ($n = 3$).

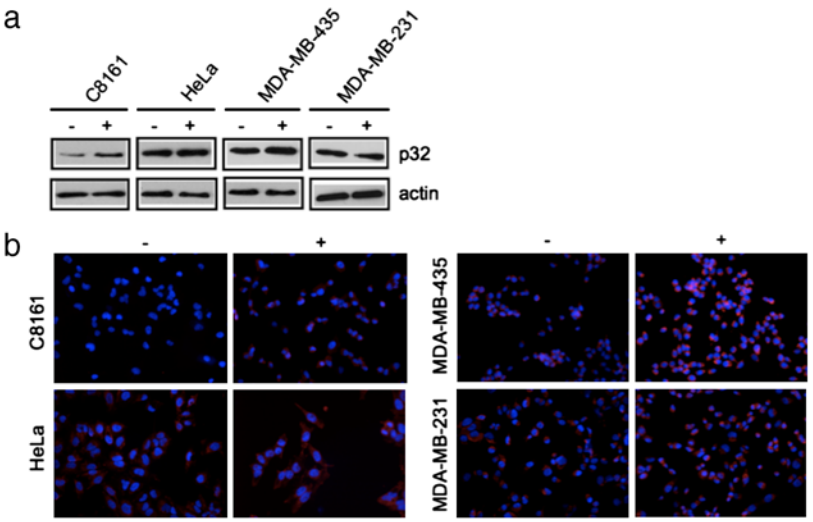

Fig. S2. Effect of p32 expression in various cultured cells on increased temperature. (*A*) Immunoblots of p32 expression on various cultured cells at increased temperature. C8161, HeLa, MDA-MB-435, and MDA-MB-231 cells were treated for 20 min at 37 °C or 45 °C (in cell incubator) and then incubated for an additional 2 h at 37 °C. β-actin was used as a control. (*B*) Fluorescence images of p32 expression on the surface of various cultured cells at increased temperature by immunostaining. The experimental procedure was the same as in (*A*). For immunostaining, after washing cells with PBS three times, the cells were fixed with 4% paraformaldehyde for 20 min, and blocked with the solution containing 1% BSA in PBS for 30 min, incubated with 5 μg/mL anti-p32 antibody for 1 h, and then with 5 μg/mL Alexa Fluor® 594 goat anti-rabbit IgG antibody for 1 h at room temperature. The nuclei stained with DAPI were observed in blue channel (excitation at 360 nm/emission at 460 nm). The p32 were observed in Cy3.5 channel (excitation at 580 nm/emission at 620 nm). Symbols – and + indicate no heating (37 °C) and heating (45 °C), respectively.

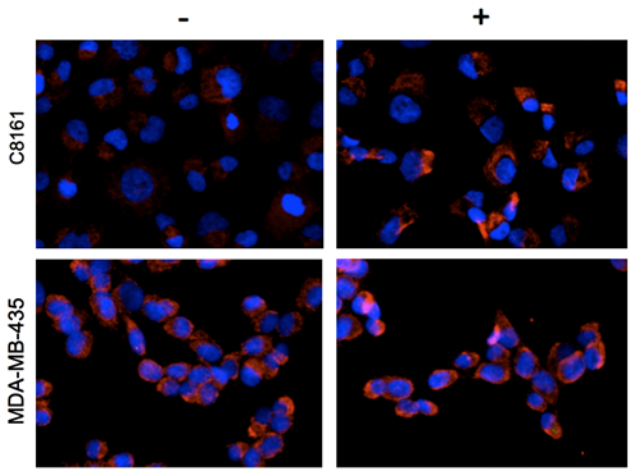

Fig. S3. In vitro cellular binding and internalization of Cy5.5-labeled control magnetic nanoworms (NWs) upon heating. C8161 or MDA-MB-435 cells were treated with NWs (*Green*) for 20 min at 37 °C or 45 °C (in cell incubator) and then incubated for an additional 2 h at 37 °C. The Cy5.5 fluorescence of NWs was imaged to observe cellular distribution of nanoparticles. The nuclei and p32 were stained with 4′-6-diamidino-2-phenylindole (DAPI, blue), and anti-p32 antibody followed by Alexa Fluor® 594 goat anti-rabbit IgG (*Red*), respectively. Symbols − and + indicate no heating (37 °C) and heating (45 °C), respectively. Brightness and contrast have been adjusted across the whole image.

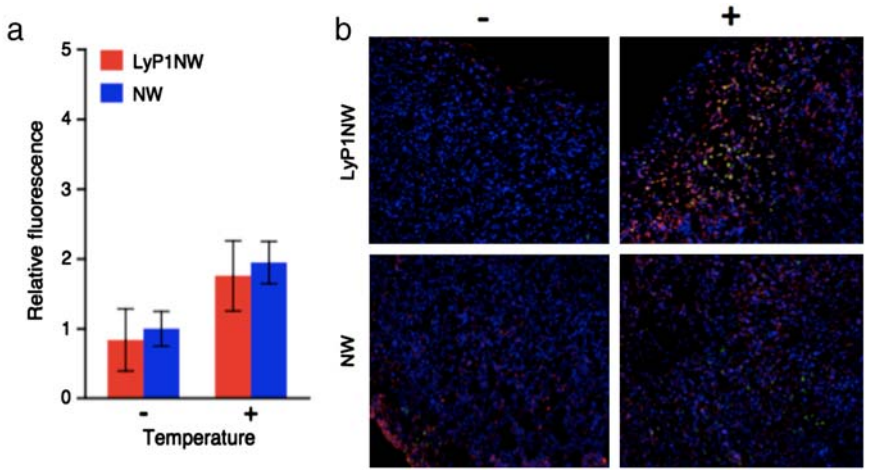

Fig. S4. (*A*) Quantification of C8161 tumor targeting of Cy7-labeled LyP-1-conjugated magnetic nanoworms (LyP1NWs) over Cy7-labeled control magnetic nanoworms (NWs) upon heating. Mice bearing bilateral C8161 tumors were intravenously injected with LyP1NWs or NWs and one tumor was immediately heated at 45 °C for 30 min using temperature-controlled water bath. At 24 h post-injection, the tissues were collected from the mice and the Cy7 fluorescence in tissues was obtained using NIR fluorescence imaging system. ($n = 3$–4). (*B*) Histological analysis of LyP1NW and NW distribution in C8161 tumors treated with or without heating. Mice bearing bilateral C8161 tumors were intravenously injected with LyP1NWs or NWs and one tumor was immediately heated at 45 °C for 30 min using temperature-controlled water bath. At 24 h post-injection, the tissues were collected from the mice, stained and imaged using fluorescence microscope. The NWs (*Green*) was labeled with Cy5.5 to determine nanoparticle distribution with Cy5.5 fluorescence in tumors. The nuclei and p32 were stained with 4′-6-diamidino-2-phenylindole (DAPI, *Blue*), and anti-p32 antibody followed by Alexa Fluor® 594 goat anti-rabbit IgG (*Red*), respectively. Symbols − and + indicate no heating (37 °C) and heating (45 °C), respectively. Brightness and contrast have been adjusted across the whole image.

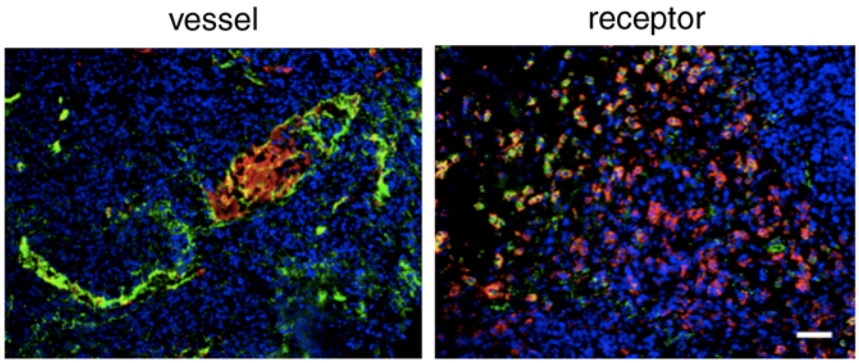

Fig. S5. Histological analysis of MDA-MB-435 tumors injected with LyP1NWs after heat treatment. Mice bearing bilateral MDA-MB-435 tumors were intravenously injected with LyP1NWs immediately after one tumor was heated at 45 °C for 30 min using temperature-controlled water bath. 24 h post-injection, the tissues were collected from the mice, stained and imaged using fluorescence microscope. The NWs (*Green*) were labeled with Cy5.5 to determine nanoparticle distribution with Cy5.5 fluorescence in tumors. The nuclei and p32 receptor or blood vessels were stained with 4′-6-diamidino-2-phenylindole (DAPI, *Blue*), and anti-p32 antibody followed by Alexa Fluor® 594 goat anti-rabbit IgG (*Red*) or CD31 followed by Alexa Fluor® 594 goat anti-rat IgG (*Red*), respectively. Scale bar is 100 μm.

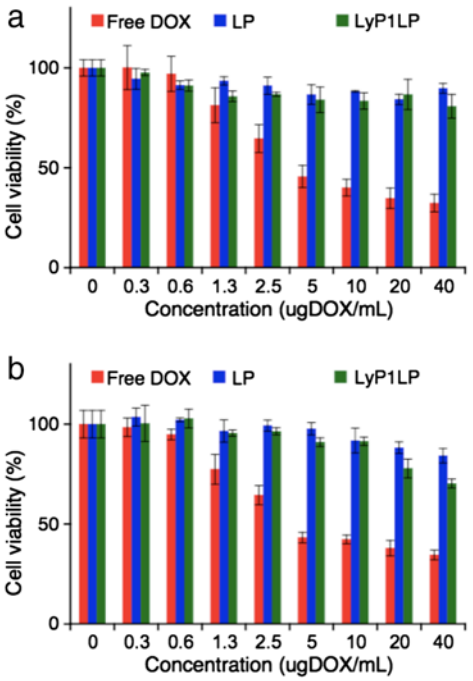

Fig. S6. Temperature-induced cytotoxicity of various therapeutic molecule or nanoparticle formulations towards C8161 human carcinoma cells by MTT assay. The cells were treated with free DOX, control DOX liposomes (LPs), and LyP-1-conjugated DOX liposomes (LyP1LPs) with different concentrations at 37 °C (*A*) or 45 °C (*B*) for 20 min (in cell incubator) and then incubated for an additional 4 h at 37 °C. The cells were rinsed with cell medium three times, incubated for an additional 44 h at 37 °C and then evaluated for cytotoxicity using MTT assay.

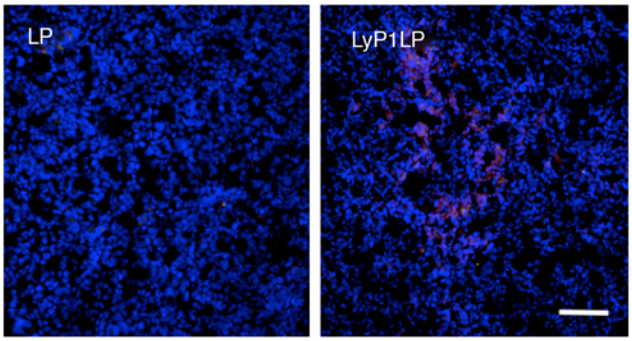

Fig. S7. Histological analysis of DOX distribution in untreated MDA-MB-435 tumors (NR-L) of the mice in fig. 4*A*. The Alexa Fluor® 488 label (on control LP, *Green*) or 5(6)-carboxyfluorescein (FAM) label (on LyP-1 of LyP1LP, *Green*) and DOX (*Red*) fluorescence of nanoparticles was imaged to determine nanoparticle and DOX distribution in tumors, respectively. The nuclei were stained with 4′-6-diamidino-2-phenylindole (DAPI, *Blue*). Scale bar is 100 μm.

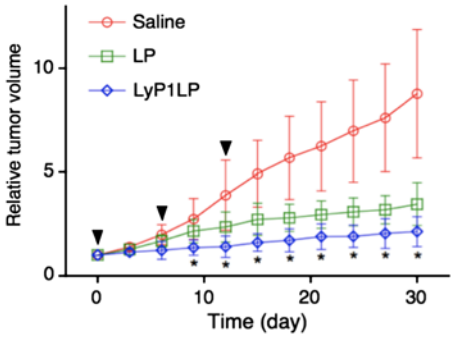

Fig. S8. Tumor therapy without photo-thermal heating. Mice bearing bilateral MDA-MB-435 tumors were injected with saline, control LPs or LyP1LPs (6 mgDOX/kg) at 0, 6, and 12 days (arrow head). Tumor volumes were monitored every 3 days after LP injection. Error bars indicate standard deviations from more than three measurements. $*P < 0.05$ for LyP1LP sample and all other treatment sets ($n = 4$).

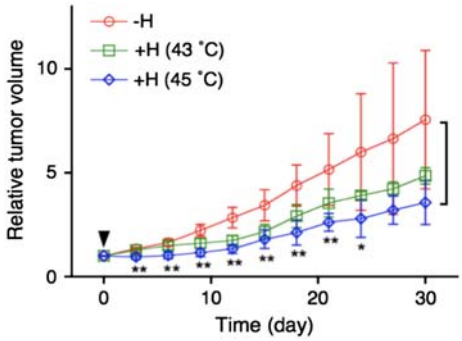

Fig. S9. NR-mediated photothermal tumor therapy at different temperatures. At 72 h post-injection of NRs (10 mgAu/kg), one tumor of the mice bearing bilateral MDA-MB-435 tumors was irradiated (810 nm, ~0.70 or ~ 0.75 W/cm^2 for 43 °C or 45 °C, respectively) for 30 min while maintaining average tumor surface temperature at ~43 or ~45 °C under infrared thermographic suirveilance. The control group was not irradiated. Tumor volumes were monitored every 3 days after irradiation. Error bars indicate standard deviations from more than three measurements. −H and +H indicate treatment without and with NR-mediated heating, respectively. $*P < 0.05$, $**P < 0.01$ for +H (45 °C) sample and −H sample ($n = 4$).